Characterization of Atmospheric Noise in the Loran-C Band

Manish Lad, Frank van Graas, Curtis Cutright, and David W. Diggle
Avionics Engineering Center, Ohio University

ABSTRACT

The signal-to-noise ratio (SNR) of the received Loran-C signal is one of the key factors in determining the usefulness of Loran-C signals for navigation. The presence of increased levels of atmospheric noise can greatly impact the received SNR of Loran signals. This increased noise can be attributed to several factors such as thunderstorms, precipitation static (p-static), and man-made interference sources. Atmospheric noise caused by lightning discharges in thunderstorms is the dominant form of noise in the Loran band.

The purpose of this paper is to characterize noise affecting system performance in different weather conditions using ground and aircraft radio frequency (RF) data collected from both wire (E-field) and loop (H-field) antennas. Modeling of the noise environment will help determine if new receiver technology or Loran-C station improvement can make Loran-C achieve the accuracy, availability, integrity, and continuity standards for Required Navigation Performance (RNP) 0.3.

1. INTRODUCTION

LOng RAnge Navigation or Loran-C is a ground-based, hyperbolic radionavigation system operating in the radio frequency (RF) spectrum of 90 to 110 kHz. The system is not line-of-sight dependent and the power radiated from the transmitters ranges from 200 kilowatts (kW) to 2 Megawatts (MW). Such complementary properties of Loran-C compared to the Global Positioning System (GPS) and the vulnerability of GPS to interference and jamming has led to evaluation of the current and potential capabilities of Loran-C to augment GPS [5]. The improved infrastructure of Loran-C transmitters and receivers capable of acquiring all stations in view simultaneously are some of the recent developments providing increased Loran-C capability. Research has also focused on using the Loran-C signal as a carrier for information like DGPS correction data, GPS-status information, or Loran-C correction data [6]. Thus, Loran-C can be used as a redundant source for GPS integrity information.

Loran-C is the third version of Loran developed since World War II and was designed for maritime users along the U.S. coasts and, later on in the Great Lakes region. The current system now provides navigation, location, and timing services for both civil and military air, land and marine users. Loran-C is approved as an en route supplemental air navigation system for both Instrument Flight Rule (IFR) and Visual Flight Rule (VFR) operations [8].

2. LORAN-C BACKGROUND

This section briefly describes the Loran-C signal and its characteristics as specified in reference 1. For a more detailed description of the signal specification and propagation characteristics, the reader is again referred to reference 1.

The basic Loran-C system consists of a chain of three or more transmitters. Each chain has a designated Master station (M) and two-to-five Secondary stations, designated as Victor (V), Whiskey (W), Xray (X), Yankee (Y), and Zulu (Z). There are ten such chains providing coverage in the contiguous United States. Each chain has its own unique repetition interval called the Group Repetition Interval (GRI). The Master and Secondary stations broadcast radio pulses at precise time intervals. The Secondary stations emit a set of eight pulses in alphabetical order of their letter designator after the Master has transmitted its set of nine pulses [1]. For example, the Loran-C chain covering the north-east part of United States, called the North-East U.S. (NEUS) chain, consists of a Master (M) and four Secondary stations (W, X, Y and Z).

The signal transmission is timed as follows: M emits a set of nine pulses. After the M signal reaches W, it delays its transmission for an interval called the Coding Delay (CD). The total elapsed time from the M transmission until the W transmission is termed the Emission Delay (ED) [1]. ED is the sum of propagation time of the signal from M to W plus the CD. After W transmits, X (with a specified CD/ED), transmits a set of eight pulses. Similarly, Y and Z transmit in sequence. The sequence is completed when the Master (M) again starts the transmission of nine-pulse group [1]. Coding delays are selected such that there are no signal overlaps within a particular chain coverage region. Some stations have only one function (i.e., to serve as a Master or Secondary in a particular chain), but other transmitters are "dual-

rated", meaning that they serve as the Master in one chain, and the Secondary for a neighboring chain [1].

2.1 Loran-C Operation

Each transmitter in the Loran-C chain broadcasts a sequence of pulses within a 20 kHz bandwidth centered around 100 kHz. A pulse is approximately 250 μsec long and the carrier envelope of each pulse rises from zero to maximum amplitude within 65 μsec and then decays for the rest of the pulse duration. A normal pulse with zero-degree carrier phase is shown in Figure 1. The positive-going third zero crossing at 30 μsec is used as the tracking point. The amplitude of the envelope at 25 μsec is used for calculating the signal strength. The Signal-to-Noise Ratio (SNR) is calculated by using the ratio of the signal strength and the noise level present in the 20-kHz bandwidth.
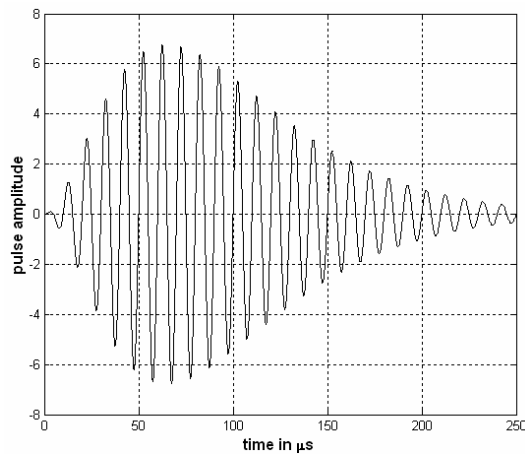
Figure 1. Loran-C pulse

A Master station transmits a series of nine pulses; the first eight pulses are spaced 1 msec apart, while the ninth pulse is spaced 2 ms apart from the eighth pulse. Secondaries transmit a series of eight pulses which are spaced 1 msec apart. The time interval between the successive transmission of a set of pulses is termed the Group Repetition Interval (GRI). The GRI is expressed in microseconds and each Loran-C chain has a unique GRI. The GRI divided by 10 is often used to identify a Loran-C chain. The phase of successive pulses in a group of 8 or 9 pulses is not the same, but the phase pattern of each group repeats every Pulse Code Interval (PCI), which is twice the duration of the GRI. Transmitters incorporate Cesium clocks as standard equipment and the timing is synchronized to Universal Time, Coordinated (UTC) (within 100 μsec). The transmitters are monitored by the U.S. Coast Guard, operator of the system, and

associated Loran-C monitor sites are used to detect any anomalous or out-of-tolerance conditions [1].

2.2 Position determination using Loran-C

Each Loran station transmits a set of pulses at precise time intervals. A receiver measures the difference in time-of-arrival of the Master and the various Secondary signals from the same chain (i.e., same GRI). This interval is termed as a time-difference-of-arrival (TD). The locus of points having the same TD from a specific Master-Secondary pair is a hyperbolic line-of-position (LOP) [1]. At least two LOPs are required to determine the position of a user. Figure 2 depicts the NEUS chain (GRI: 9960) that a receiver in the north-east part of the U.S. might receive. The received signal amplitude of a transmitting station depends on the transmitter power, the distance of the receiver from the station, and the propagation characteristics of the path traveled by the signal.
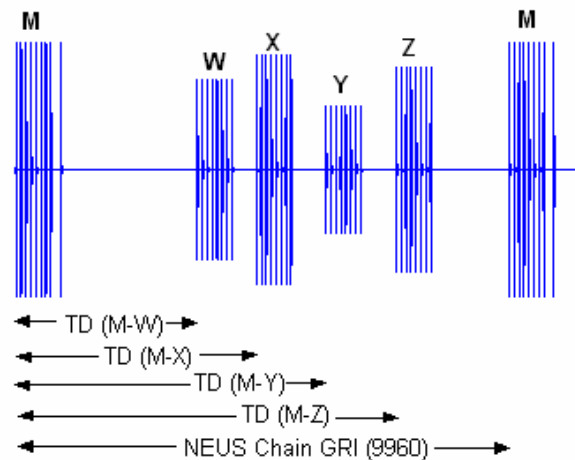
Figure 2. Received pulse pattern for the NEUS chain

2.3 Loran-C propagation

The speed of propagation of the Loran-C signal depends on the conductivity and permittivity of the surface over which it travels. The speed of propagation of the Loran-C signals must be corrected as a function of the terrain and/or water over which the signal travels. The Primary Phase Factor (PF), Secondary Phase Factor (SF), and Additional Secondary Phase Factor (ASF) account for changes in propagation speed due to air, seawater, and land paths, respectively [1]. Accurate modeling of the ASF values is required for precise navigation and positioning if propagation over land is involved.

There are two paths by which Loran-C signals propagate. The ground wave signals propagate in the atmospheric medium below the ionosphere along the Earth's surface. The Loran-C signals can also propagate as sky waves reflecting from the ionosphere. Sky waves are not desirable for accurate navigation since the propagation conditions in the ionosphere are not stable [1]. Sky-wave contamination can affect the position solution obtained using the Loran-C ground-wave signal.

2.4 Interference

Interference caused by transmissions from other chains is termed cross-rate interference. Pulses from transmitters within a particular chain do not overlap as explained in Section 2.2. However, transmissions from different chains are not synchronous and can therefore, occasionally overlap with the desired pulses. Interference can also be caused by narrow-band (NB) or continuous wave (CW) transmissions in or near the Loran-C band (90-110 kHz).

3. Flight Test Equipment Set-Up

This section provides a brief overview of the equipment used in the flight tests, for collecting the data used for analysis and characterization of atmospheric noise.

The set up used to collect the airborne Loran-C data is comprised of the following components:

1) LORADD-DS DataGrabber
   The DataGrabber is a part of the data collection equipment (shown in figure 4); it is used for collecting the Loran-C data.
   Sampling rate: 400 kHz, Resolution: 16 bits
   Two input channels-samples simultaneously
   Dynamic Range: 96 dB
2) WX-500 Stormscope
   The Stormscope is used for determining the approximate distance of the aircraft from the thunderstorm.
3) NovAtel OEM4 GPS WAAS receiver
   The GPS receiver is primarily used for providing the position and time for data processing. It is a component of the data collection equipment.
4) Apollo 618 (Loran-C Receiver)
   The Loran-C receiver is used to power the E-field antenna.
5) E-field (Wire) Antenna
   The wire antenna is mounted on the top of the fuselage of the aircraft. The wire antenna is a II-morrow, Inc. (UPS Aviation Technologies),

model A-16 whip antenna with integral preamplifier.
6) H-field (Loop) Antenna
   The loop antenna is mounted on the bottom of the aircraft. The antenna is a dual-loop King Radio KA-42A Automatic Direction Finding (ADF) antenna.
7) Data Collection Computer

The King Air, shown in Figure 3 was used for collecting the airborne data.

Figure 3. Flight Test Aircraft (King Air)

The block diagram of the aircraft equipment set-up is shown in Figure 4.
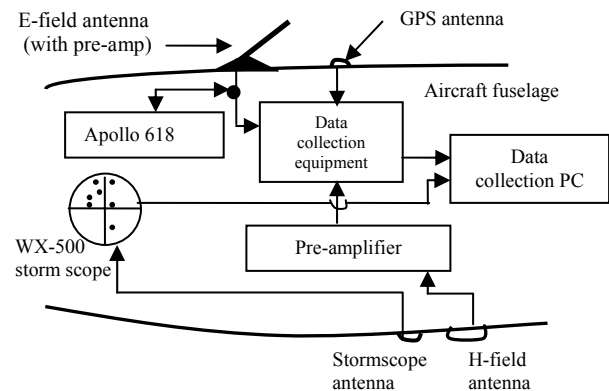
Figure 4. Flight Test Equipment Block Diagram

For a detailed description of the equipment set-up, the reader is referred to reference 3.

4. Data Processing

The data collected using the DataGrabber is processed in 2-sec blocks (see Figure 5). To characterize atmospheric noise, first, the Narrow-Band (NB) and Continuous Wave (CW) interference present in the signal along with any thunderstorm bursts are removed. Loran-C pulses that are above the noise

floor are also removed, so that only atmospheric noise remains.
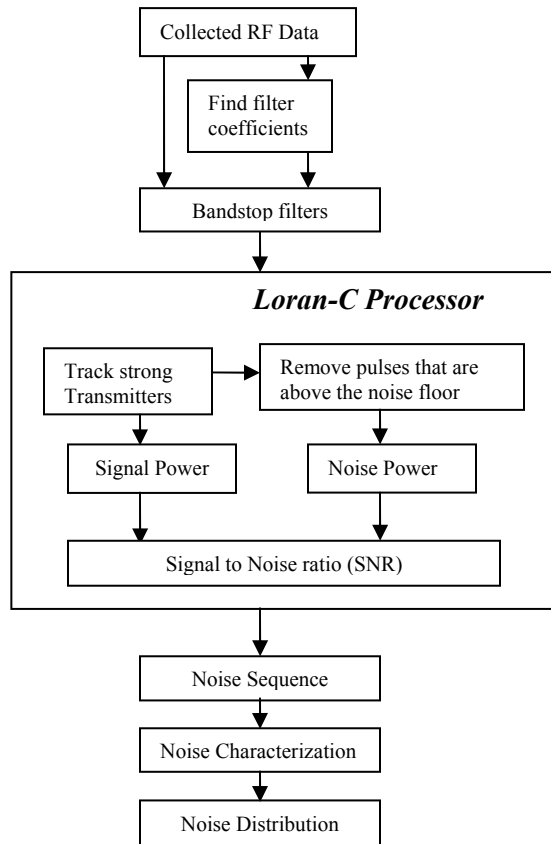
Figure 5. Data Processing Overview

Signal-to-noise ratio (SNR) is computed for each transmitter whose signal amplitude is well above the noise floor. SNR is a function of user location as well as atmospheric noise. SNR in this paper is calculated as the SNR value measured at the output of the antenna.

Figure 6 shows the detailed diagram of the data processing. CW and NB interference detection is performed by passing the signal through a bank of band-pass filters, each with a bandwidth of 500 Hz, and squaring the output of the filters. After identifying a potential interference source, it is filtered from the signal using a bandstop filter.

Thunderstorm bursts have a high energy level compared to the noise floor. To remove noise bursts caused by such conditions, the signal energy is calculated in time-bins and a time-bin is discarded if the bin has energy above a set threshold. At this point in the processing, the signal contains Loran-C pulses and noise. The signal is integrated over the PCI of the Loran chain and the stations with signal amplitude

above the noise floor are identified using the user position.
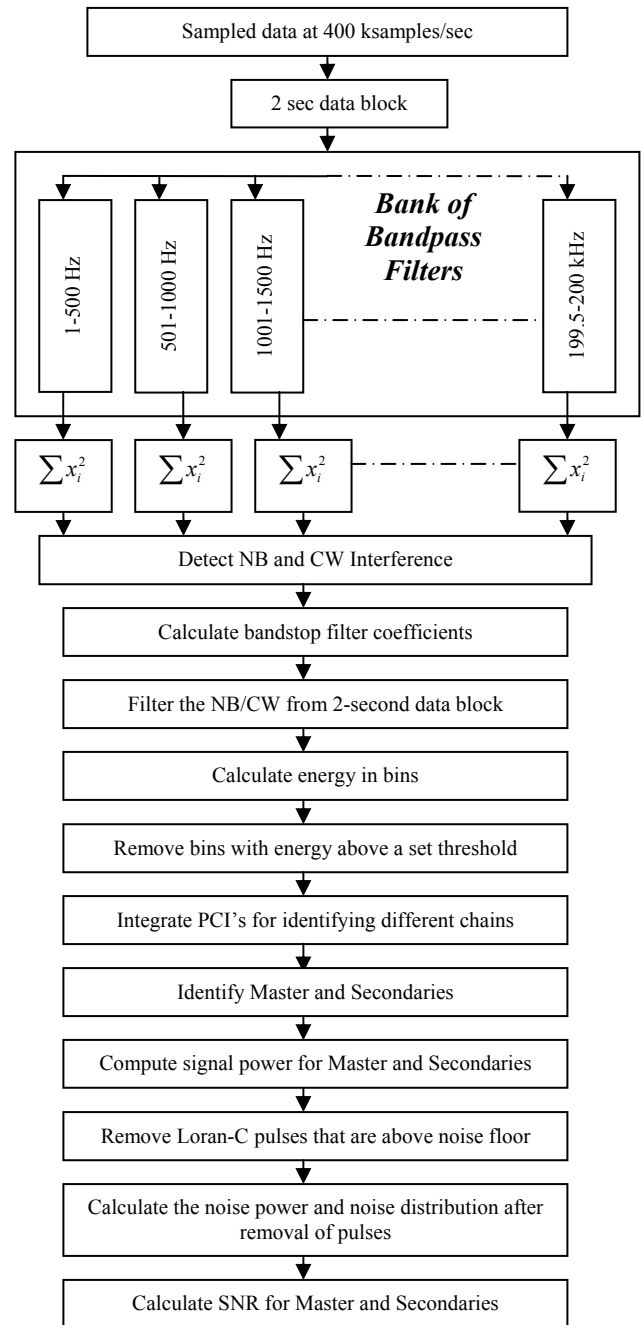
Figure 6. Data Processing

Samples that contain Loran-C pulses that are above the noise floor are removed. The remaining noise sequence is used to characterize the noise and to calculate the noise distribution.

5. Flight Test Results

This section describes the results obtained from three flight experiments. The first flight experiment was flown under normal conditions in Ohio. The second and third flight experiments took place in thunderstorm conditions in Florida.

First flight experiment

Flight data near Albany, Ohio were collected on 13 August, 2003 from 08:54:42 to 09:00:06 local time. Figure 7 illustrates the trajectory obtained from GPS.

Figure 7. Trajectory for the first flight experiment

Since the North-East U.S. chain provided better coverage than any other chain for the given flight trajectory, SNR values for the NEUS chain transmitters were calculated. Figure 8 shows the Loran-C transmitter locations in the NEUS chain. The Master (located in Seneca, NY) and the Z Secondary (located in Dana, IN) provided good signal strengths and thus were used for SNR calculations.
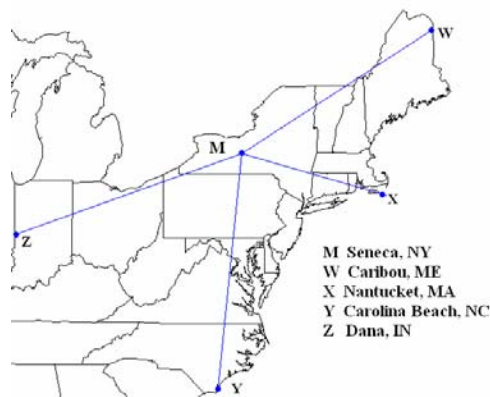
Figure 8. North-East U.S. Loran-C chain

E-field Results

The top plot in Figure 9, shows the raw data collected from one of the channels (E-field antenna channel) of the DataGrabber and the bottom plot illustrates the signal after integrating over the PCI for the NEUS chain (after eliminating NB/CW interference). Signal amplitudes are expressed in A/D level, which can range between -32,767 and +32,768.
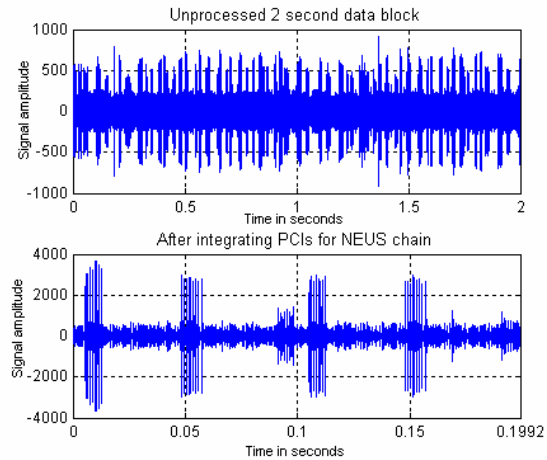
Figure 9. E-field antenna channel unprocessed 2-second data block (top plot) and results after integrating over the PCI for the NEUS chain (bottom plot) for the first flight experiment

Two occurrences of the Master and two occurrences of the Z Secondary are visible in the bottom plot of Figure 9. However, only occurrence of the Y Secondary is present. Therefore, only the SNR values of M and Z are computed. Figure 10 below shows the processing results.
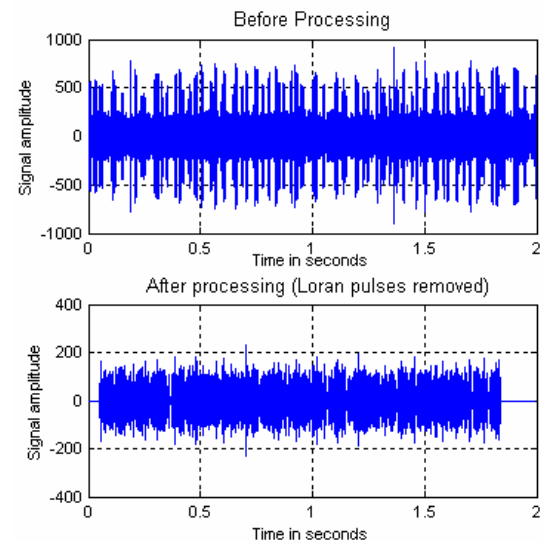
Figure 10. E-field antenna channel before (top plot) and after (bottom plot) removal of Loran-C pulses that are above the noise floor for the first flight experiment

The top plot of Figure 10 shows the received signal before removal of the Loran-C pulses, while the

bottom plot shows the noise sequence after removal of the Loran-C pulses.

Note that all Loran-C pulses that are above the noise floor are removed. In this example, it includes all the secondary stations from the NEUS chain and the pulses from neighboring chains. Next, the distribution of the noise samples for the entire 326-sec data set is computed (see Figure 11). A total of approximately 13 million independent noise samples are contained in the distribution, which provide experimental data for probabilities as small as 10^{-7}.
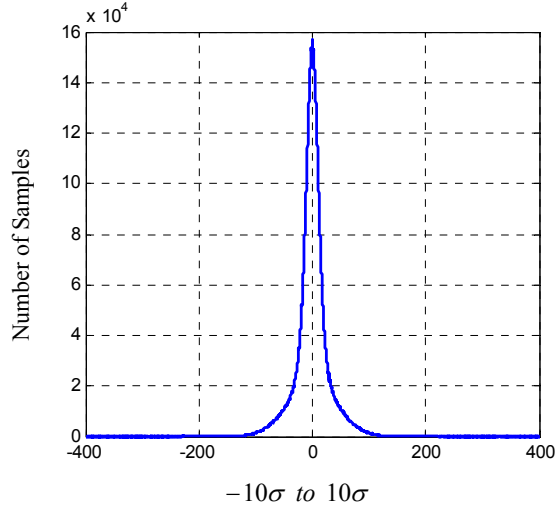
Figure 11. E-field antenna channel noise distribution for the first flight experiment

From the noise distribution, the cumulative distribution function (cdf and 1.0-cdf) of the noise is calculated and plotted against the Gaussian cdf (with the same standard deviation as the noise) in Figure 12. The plot indicates that the tail probabilities of the calculated noise cdf (and 1.0-cdf) are larger than the Gaussian cdf (and 1.0-cdf) with an equivalent rms value. The collected noise can be overbounded by a Gaussian distribution that has three times the standard deviation of the collected noise. Overbounding means that the probability of exceeding a certain noise realization is less than the corresponding probability of a Gaussian realization.

H-field Results

The data collected from the H-field antenna are processed in a similar way as those for the E-field antenna. Figure 13 illustrates the signal obtained after integrating over the PCI for the NEUS chain.

The H-field antenna path has a lower overall gain compared to that of the E-field antenna path.

Therefore, the amplitude of the signal at the output of the H-field antenna is less when compared to the E-field antenna output.
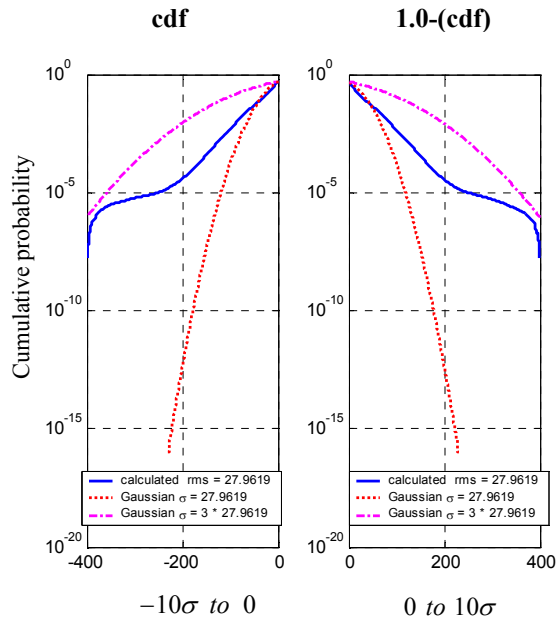
Figure 12. E-field antenna channel noise statistics for the first flight experiment
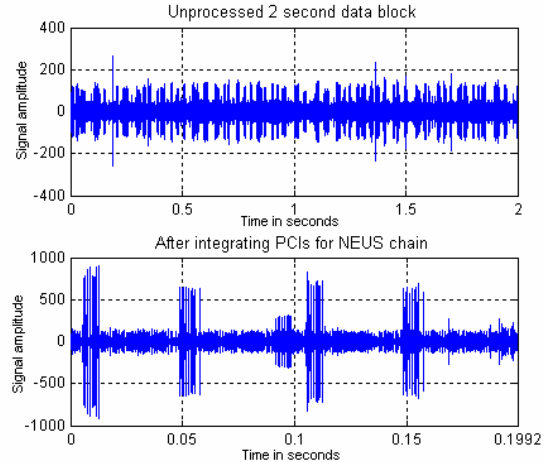
Figure 13. H-field antenna channel unprocessed 2-sec data block (top plot) and results after integrating over the PCI the NEUS chain (bottom plot) for the first flight experiment

For these tests, equal amplitudes for E-field and H-field signals were not necessary for the comparison of the performance of the two antenna systems.

The top plot of Figure 14 shows the received signal before removal of the Loran-C pulses, while the bottom plot shows the noise sequence after removal of

the Loran-C pulses, NB and CW interferences using the H-field antenna.
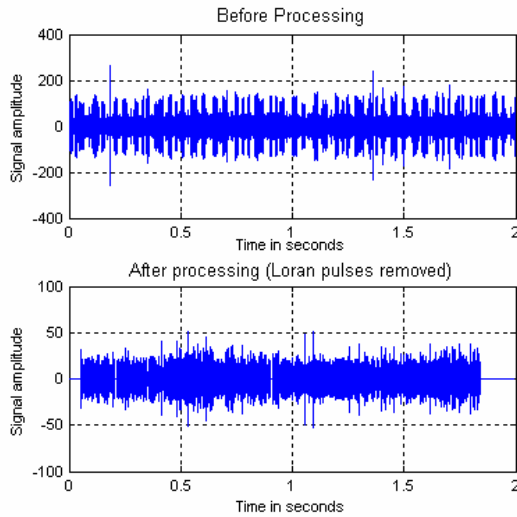
Figure 14. H-field antenna channel before (top plot) and after (bottom plot) removal of Loran-C pulses that are above the noise floor for the first flight experiment

The distribution for the H-field noise for the entire data set is shown in Figure 15.
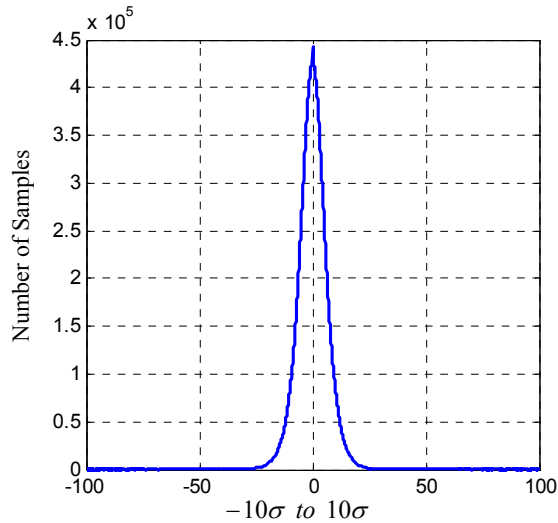
Figure 15. H-field antenna channel noise distribution for the first flight experiment

Figure 16 shows the cdf and 1.0-cdf for the H-field antenna. The cdf for the H-field antenna are almost overbounded by a Gaussian cdf with a standard deviation of three times the standard deviation of the collected noise.
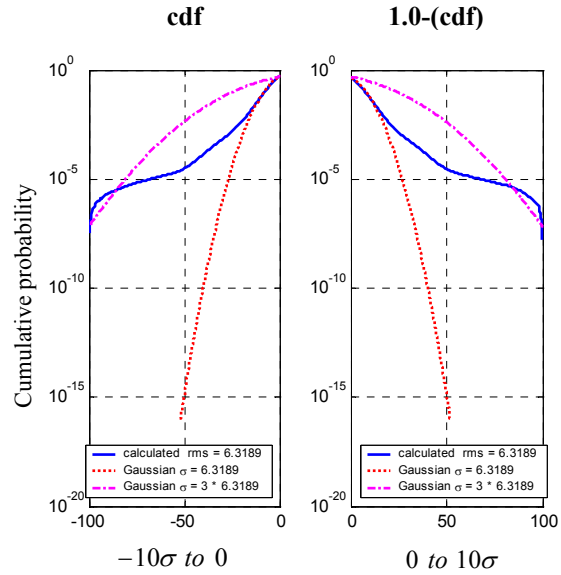
Figure 16. H-field antenna channel noise statistics for the first flight experiment

Averaged SNR values (at the output of the antenna) and the RMS values of the noise calculated after processing the collected data are provided in Table 1

Table 1. Averaged SNR measurements and RMS noise levels for the first flight experiment

Antenna	SNR M (dB)	SNR Z (dB)	RMS noise (AD count)
E-field	10.5	13.3	28
H-field	12.4	13.2	6.3

From the results in Table 1, the H-field (loop) antenna system has a slightly better SNR than the E-field (wire) antenna system.

Second Flight Experiment

The second flight test was conducted under thunderstorm conditions near Orlando, Florida on August 14, 2003 from 12:29:32 to 12:34:56 local time. Figure 17 shows the flight trajectory obtained from GPS.

Figure 17. Trajectory for the second flight experiment

The South-East U.S. chain (SEUS) was used for the SNR calculations. Figure 18 shows the SEUS chain transmitter locations.
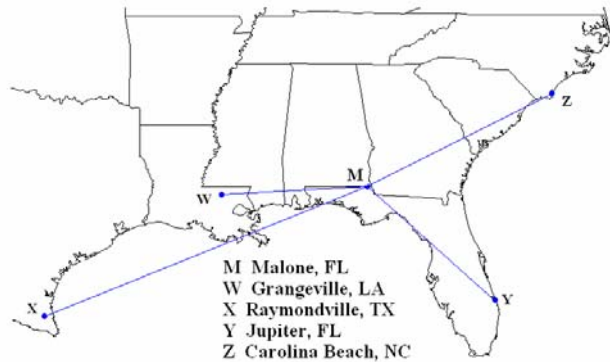
Figure 18. South-East U.S. Loran-C chain

E-field Antenna Results

The airborne data were collected in the vicinity of thunderstorms. Figure 19 shows one such instance where the 2-sec data block was affected by lightning discharges from a thunderstorm. The thunderstorm noise burst in this case had large amplitude over a short period of time.
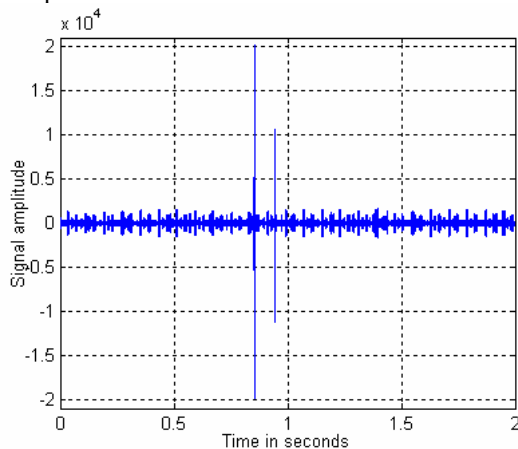
Figure 19. E–field antenna data example with short-duration, large amplitude lightning noise

The top plot of Figure 20 shows the received signal with the short-duration lightning noise before removal of the Loran-C pulses, while the bottom plot shows the noise sequence after removal of the Loran-C pulses, NB and CW interferences and lightning noise. The RMS noise floor in this case is higher by a factor of approximately 1.7 compared to the noise floor obtained in the first flight experiment.
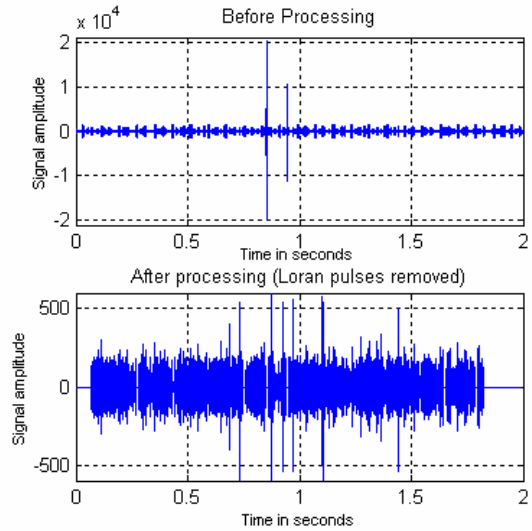
Figure 20. Short-duration lightning noise for the E-field antenna before (top plot) and after (bottom plot) removal of lightning noise, NB, CW, and Loran-C pulses that are above the noise floor for the second flight experiment

Figure 21 depicts a scenario where the thunderstorm had sustained energy over a larger time interval. In this case, the received amplitude of the strike was smaller compared to Figure 19, but the energy was present for a longer period of time.
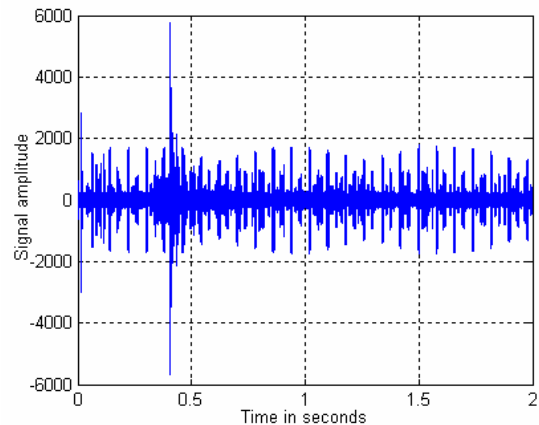
Figure 21. E–field antenna data example with longer-duration, high-energy lightning noise

The top plot of Figure 22 shows the received signal with the high-energy lightning noise before removal of the Loran-C pulses, NB and CW interferences while the bottom plot shows the noise sequence after removal of the Loran-C pulses and lightning noise.
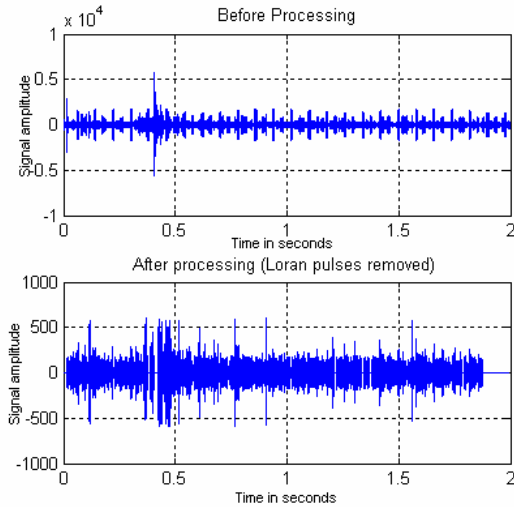
Figure 22. Lightning noise for the E-field antenna before (top plot) and after (bottom plot) removal of lightning noise, NB, CW and Loran-C pulses that are above the noise floor for the second flight experiment

The noise distribution for the entire 326-sec data set is shown in Figure 23. The peak in the center of the distribution is due to a large number of samples that have a value close to zero. The reason for this peak is under investigation.
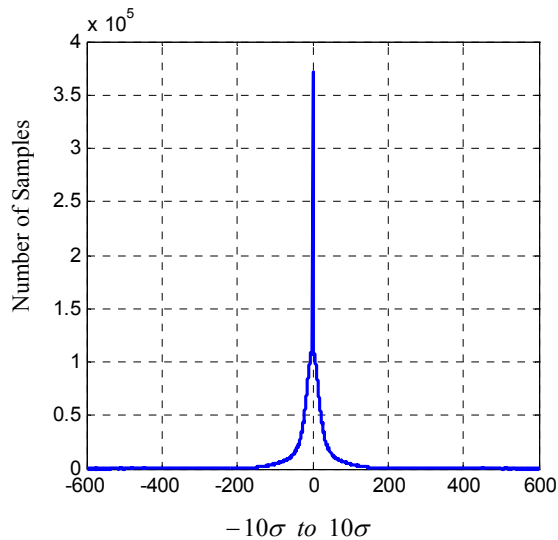
Figure 23. E-field antenna channel noise distribution for the second flight experiment

Figure 24 shows the cdf and 1.0-(cdf) corresponding to the data presented in Figure 23. The shapes of the cdf and 1.0-(cdf) are similar to the ones obtained from the data for the first flight experiment (see Figure 12).
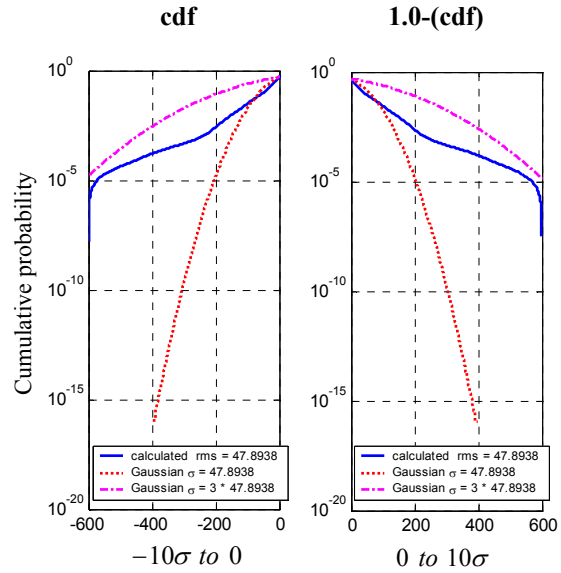
Figure 24. E-field antenna channel noise statistics for the second flight experiment

<u>H-field Antenna Results</u>

Figure 25 shows the noise distribution for the H-field antenna. This distribution also has a peak around zero due to a large number of samples with values close to zero.
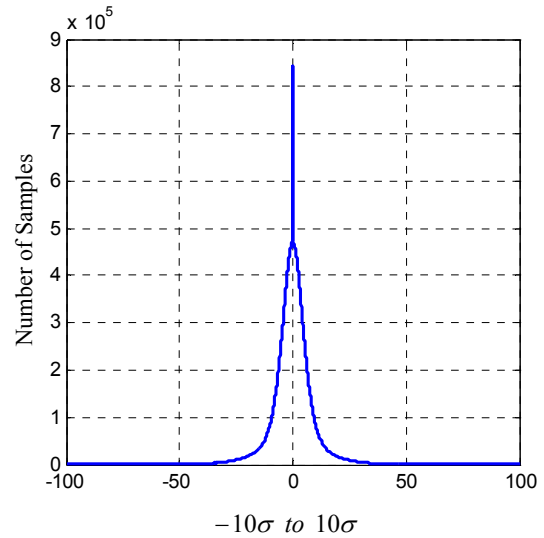
Figure 25. H-field antenna channel noise distribution for the second flight experiment

Figure 26 shows the cdf and 1.0-(cdf) for the H-field antenna. Again, the shape of the cdf and 1.0-(cdf) are similar to the ones obtained from the first flight experiment (see Figure 16).

cdf **1.0-(cdf)**

$-10\sigma\ to\ 0$ $0\ to\ 10\sigma$
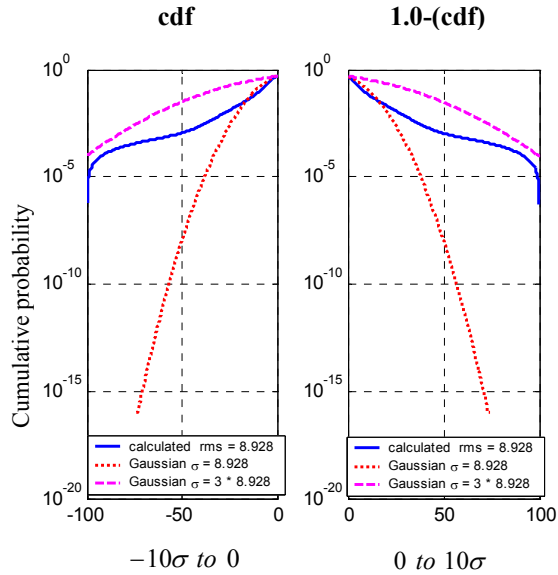
Figure 26. H-field antenna channel noise statistics for the second flight experiment

Averaged SNR measurements for Master (Malone, FL) and Y Secondary (Jupiter, FL) along with RMS values of the noise for the entire 326-sec data set are shown in Table 2.

Table 2. Averaged SNR measurements and RMS noise levels for the second flight experiment

Antenna	SNR M (dB)	SNR Y (dB)	RMS noise (AD count)
Wire	7.4	8.8	48
Loop	8.6	12.1	9

Third Flight Experiment

The third flight test was conducted under thunderstorm conditions (mild compared to the previous one) near Palm Coast, Florida on August 14, 2003 from 12:56:44 to 13:02:08 local time. Figure 27 shows the flight trajectory obtained from GPS.
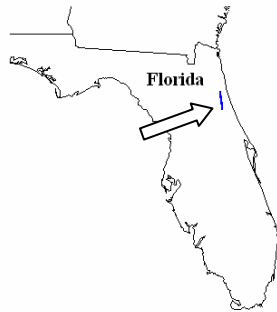
Figure 27. Trajectory for the third flight experiment

This flight experiment also used the SEUS Loran-C chain.

E-field Antenna Results

The E-field noise distribution is shown in Figure 28. The noise distribution for this data set also has a peak around zero.

$-10\sigma\ to\ 10\sigma$
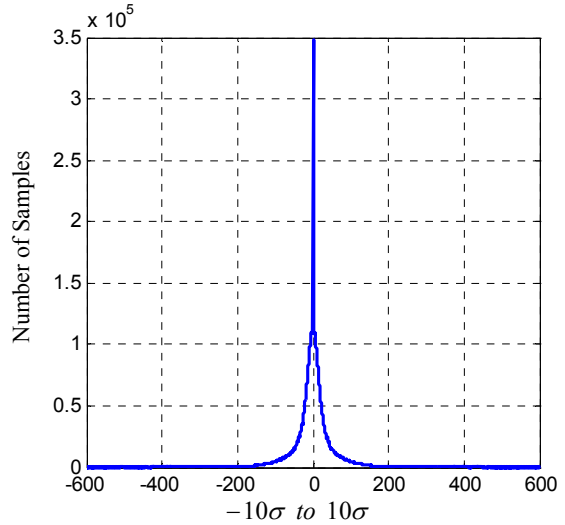
Figure 28. E-field antenna channel noise distribution for the third flight experiment

The cumulative distribution functions cdf and 1.0-(cdf) for the E-field antenna are shown in Figure 29.

cdf **1.0-(cdf)**

$-10\sigma\ to\ 0$ $0\ to\ 10\sigma$
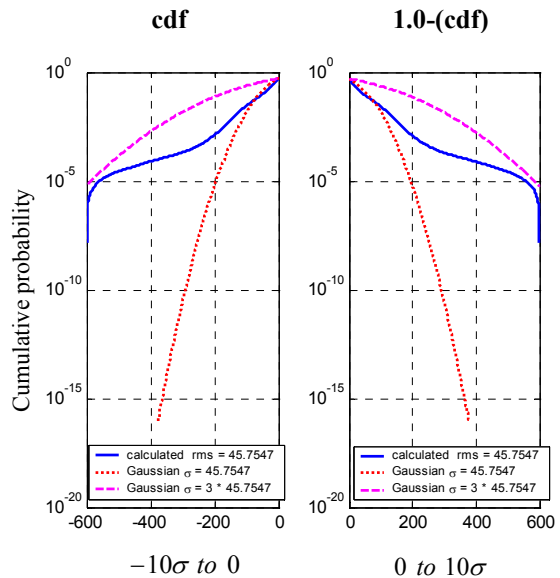
Figure 29. E-field antenna channel noise statistics for the third flight experiment

H-field Antenna Results

Figure 30 shows the noise distribution for the H-field antenna.

x 10⁵ chart — Number of Samples vs -10σ to 10σ
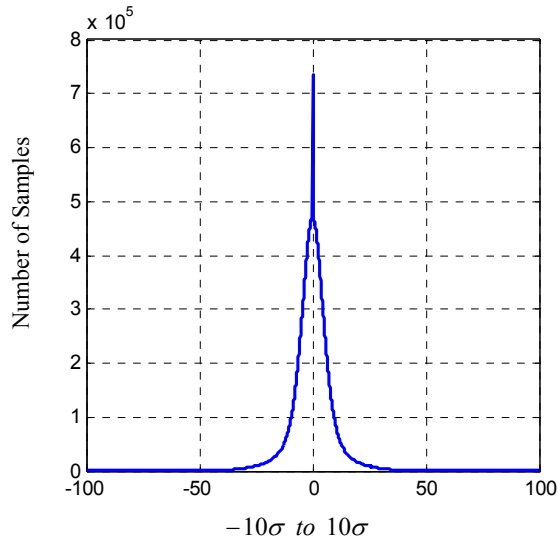
Figure 30. H-field antenna channel noise distribution for the third flight experiment

Figure 31 shows the cdf and 1.0-(cdf) corresponding to Figure 30 for the H-field antenna.

cdf and 1.0-(cdf) plots with legend:
calculated rms = 8.6961
Gaussian σ = 8.6961
Gaussian σ = 3 * 8.6961

-10σ to 0 0 to 10σ
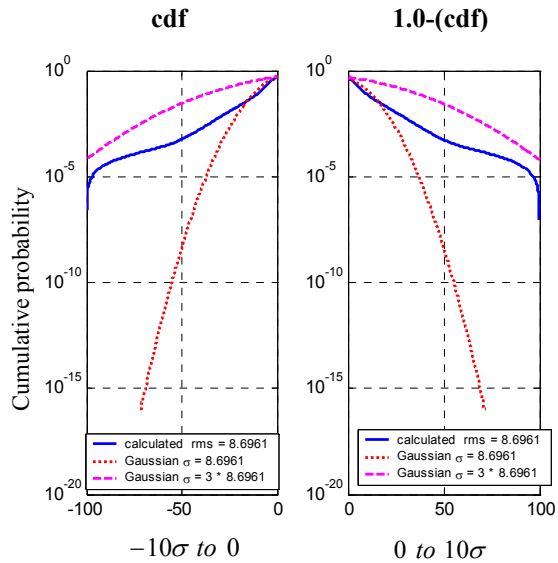
Figure 31. H-field antenna channel noise statistics for the third flight experiment

Averaged SNR measurements and the RMS values of noise for the entire 326-sec data set are shown in Table 3.

Table 3. Averaged SNR measurements and RMS noise levels for the third flight experiment

Antenna	SNR M (dB)	SNR Y (dB)	RMS noise (AD count)
Wire	12.6	15.2	46
Loop	13.8	18.4	8.7

From Table 3, it follows that the RMS noise values are only slightly smaller than those experienced during the second flight experiment (see Table 2). The SNR values for the Master at Malone and Y Secondary at Jupiter are between 5 and 7 dB higher than for the second flight experiment. The reasons for this relatively large increase in signal strength are under investigation.

Conclusions

From the preliminary results presented in this paper, the following conclusions are derived:

1. The cores of the atmospheric noise distributions for both E-field and H-field antenna channels resemble Gaussian distributions.
2. The tail probabilities of both E-field and H-field antenna channel atmospheric noise can be overbounded by a Gaussian distribution with a standard deviation of 3 times that of the collected data. Experimental data based on a sample size of approximately 13 million independent samples, support these overbounds for probabilities as small as 10^{-6} to 10^{-7}.
3. The shapes of the cumulative distribution functions for both E-field and H-field antenna channels, under various atmospheric noise conditions experienced in flight, are similar.

Additional flight test experiments are planned to evaluate atmospheric noise characteristics under different weather conditions.

Acknowledgements

References

1. LORAN-C User Handbook, COMDTPUB P16562.6, November 1992

2. Van Graas, D.H. and Van Graas, F., "Aircraft Loran-C Dual-Loop Antenna System Design and Flight Test," Proceedings of the National Technical Meeting of the ION, San Diego, California, January 22-24, 2001.

3. Cutright, C., et al., "Loran-C Band Data Collection Efforts at Ohio University," Proceedings of the International Loran Association (ILA-32) Convention and Technical Symposium, Boulder, Colorado, November 3-7, 2003.

4. Lo, S., et al., "The Loran Integrity Performance Panel (LORIPP)," Proceedings of ION-GPS, Satellite Division of the ION, Portland, Oregon, September 24-27, 2002.

5. "Vulnerability Assessment of the Transportation Infrastructure Relying on the Global Positioning System", John A. Volpe National Transportation System Center, August 20, 2001.

6. Offermans G. and Helwig A., "Integrated Navigation System Eurofix - Vision, Concept, Design, Implemenation and Test", 2003

7. Department of Transportation, United States Coast Guard, "Specification of the transmitted Loran-C Signal," Report COMDTINST M16562.4, Washington, D.C., July 1981.

8. Department of Defense and Department of Transportation, 1999 Federal Radionavigation Plan, February 2000.